2009 American Control Conference
Hyatt Regency Riverfront, St. Louis, MO, USA
June 10-12, 2009

Control of underactuated undulatory locomotor exploiting anti-resonance: A case study

R. Forch and T. Iwasaki

Department of Mechanical and Aerospace Engineering
University of Virginia, 122 Engineer's Way
Charlottesville, VA 22904-4746
Email: {raf8v,iwasaki}@virginia.edu

Abstract

Rhythmic movements in animal locomotion appear to exploit a resonance of the body-environment dynamics to maintain high efficiency. To gain insights into the locomotion mechanism, this paper studies a simple three-link undulatory locomotor model that swims through a single joint torque actuator. We have found that, when the locomotor is driven by a sinusoidal input of a given amplitude, the resulting locomotion speed is maximum when the driving frequency is close to the anti-resonance of the link chain. We then show how the anti-resonance can be exploited in the feedback control based on central pattern generators.

1. Introduction

In locomotion of various animals, resonance appears to be exploited to increase efficiency. For instance, the pace of human walking would be close to a resonance frequency of the legs acting as pendulums. The biological control system, directly achieving such locomotion, is formed by a group of interconnected neurons called the central pattern generator (CPG). The CPG by itself is a nonlinear oscillator having an intrinsic phase pattern that resembles, but is slightly different from, the gait observed during locomotion [1]. It is a long standing problem in neuroscience to uncover how the CPG works as a controller in a feedback loop to generate an efficient gait.

Entrainment of CPGs to a resonance of a mechanical body has been studied in the literature [2]–[7]. Many of these results considered a one-degree-of-freedom flexible system like a pendulum, driven by a simple CPG called the reciprocal inhibition oscillator (RIO) [8]. The closed-loop system was analyzed through numerical simulations and the method of harmonic balance. It has been found [7] that the RIO is able to entrain to the mechanical resonance under certain conditions; either $\omega_{\text{CPG}} \ll \omega_{\text{RES}}$ with negative feedback, or $\omega_{\text{CPG}} \gg \omega_{\text{RES}}$ with positive feedback, where ω_{CPG} and ω_{RES} are the intrinsic frequency of the RIO and the resonance frequency of the mechanical system.

In this paper, we consider a more realistic mechanical model for locomotion. Specifically, we study a simple locomotor that is formed as a chain of three rigid links connected through flexible joints. The locomotor swims in water by undulating its body through a torque actuator placed at one of the two joints. We have found that, when the locomotor is driven by a sinusoidal input of a given amplitude, there exists a frequency at which the resulting locomotion speed is maximum. Moreover, this frequency is close to the anti-resonance, rather than a resonance, of the link chain. We then examine whether an RIO can entrain to the anti-resonance, or to one of the resonance frequencies. As expected from the previous studies of a pendulum-RIO system [6],[7], it turns out the RIO is able to entrain to a resonance, but only to the second mode that results in poor swimming. However, we further show that a phase-lag compensator, placed in the feedback loop right before the RIO, can achieve the phase balance appropriate for entrainment to the anti-resonance for efficient swimming.

2. An undulatory locomotor

Consider the chain of links depicted in Fig. 1, which consists of n links connected through $n-1$ joints (case $n = 4$ is shown). Each link is rigid with uniformly distributed mass. We consider only planar mo-

978-1-4244-4524-0/09/$25.00 ©2009 AACC

tion, and the mechanical system has $n+2$ degrees of freedom ($n-1$ for shape, 2 for position, and 1 for orientation). The i^{th} link is of mass m_i, length $2l_i$, and moment of inertia $J_i(=m_i l_i^2/3)$. The joint between the i^{th} and $(i+1)^{\text{th}}$ links has an actuator to generate torque u_i and a linear spring with stiffness k_i. Let θ_i be the angle between the link and the inertial x-axis, and denote by θ the n-dimensional vectors whose i^{th} entry is θ_i. For the center of gravity (CG) of the whole chain, the velocity is denoted by vector v having (x,y) components (v_x, v_y).

Following the development of robotic snake model in [9], we consider the case where the i^{th} link is subject to the environmental forces and torque:

$$f_{t_i} = -c_{t_i} v_{t_i}, \quad f_{n_i} = -c_{n_i} v_{n_i}, \quad \tau_i = -(\ell_i^2/3)(c_{n_i}\dot{\theta}_i)$$

where v_{t_i} and v_{n_i} are the tangential and normal components of the velocity of the link CG, and f_{t_i}, f_{n_i} and τ_i are the forces and torque generated by the interaction of the link and environment, such as the friction on the ground or the drag in fluid. The environmental forces are directionally non-uniform and, typically, the normal force is larger than the tangential force; $c_{n_i} > c_{t_i}$. For instance, the fluid force on undulatory swimmer like leeches and lampreys may be modeled as [10]

$$c_{t_i} := 5.4 c_T \ell_i \sqrt{\rho \mu \bar{v}_n d_i}, \quad c_{n_i} = c_N \rho \bar{v}_n d_i \ell_i,$$

where c_T and c_N are the drag coefficients in the tangential and normal directions, ρ and μ are fluid density and viscosity, d_i is the width of the link, and $\bar{v}_n$ is the RMS value of the normal velocity.

Nonlinear equations of motion for the link chain can be developed from the first principle as in [9]. The model can be simplified by considering the case where the locomotion is in the x direction so that v_y is small and the undulation amplitudes $|\theta_i|$ are small. Keeping up to the second order terms in θ and v_y, we have

$$\begin{bmatrix} D & \Lambda\theta & -F^{\mathsf{T}} C_n e \\ \theta^{\mathsf{T}}\Lambda^{\mathsf{T}} & e^{\mathsf{T}} C_t e + \theta^{\mathsf{T}} C_o \theta & -\theta^{\mathsf{T}} C_o e \\ -e^{\mathsf{T}} C_n F & -e^{\mathsf{T}} C_o \theta & e^{\mathsf{T}} C_n e \end{bmatrix} \begin{bmatrix} \dot{\theta} \\ v_x \\ v_y \end{bmatrix} + \begin{bmatrix} J\ddot{\theta} \\ m\dot{v}_x \\ m\dot{v}_y \end{bmatrix} = \begin{bmatrix} Bu - C^{\mathsf{T}} K C\theta \\ 0 \\ 0 \end{bmatrix} \tag{1}$$

$$\begin{aligned} &J := LML/3 + F^{\mathsf{T}} M F, \\ &D := LC_nL/3 + F^{\mathsf{T}} C_n F, \\ &\Lambda := F^{\mathsf{T}} C_o + \mathrm{diag}(F^{\mathsf{T}} C_t e), \\ &F := M^{-1} C^{\mathsf{T}} (C M^{-1} C^{\mathsf{T}})^{-1} A L, \\ &C_o := C_n - C_t, \quad e := \begin{bmatrix} 1 & \cdots & 1 \end{bmatrix}^{\mathsf{T}}, \end{aligned}$$

where m is the total mass (sum of m_i), A (respectively C) is the $(n-1)\times n$ matrix such that the (i,i) entries are one, $(i,i+1)$ entries are one (negative one), and the other entries are zero, and M, L, K, C_t, and C_n are diagonal matrices with entries m_i, l_i, k_i, c_{t_i}, and c_{n_i}, respectively. For later reference, let us define the relative angle vector $\phi := C\theta$ and body orientation angle $\theta_o := \sum \theta_i/n$.

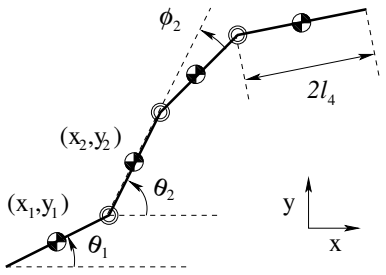

Figure 1. A link chain model for locomotor

We consider the 3-link model whose parameters are determined from measurements of a typical leech:

$$\begin{aligned} &n = 3, \quad k_o = 2\times 10^{-5}\mathrm{Nm/rad}, \\ &m = 0.0013\mathrm{kg}, \quad d_o = 0.008\mathrm{m}, \quad \ell = 0.1\mathrm{m}, \\ &\rho = 997.8\mathrm{kg/m^3}, \quad \mu = 0.001\mathrm{kg/(sm)}, \\ &c_T = 0.45, \quad c_N = 2.27, \quad \bar{v}_n = 0.03\mathrm{m/s}, \\ &A := \begin{bmatrix} 1 & 1 & 0 \\ 0 & 1 & 1 \end{bmatrix}, \quad C := \begin{bmatrix} 1 & -1 & 0 \\ 0 & 1 & -1 \end{bmatrix}, \\ &B := \begin{bmatrix} 1 & -1 & 0 \end{bmatrix}^{\mathsf{T}}. \end{aligned}$$

The body is approximated by a uniform chain with (m_i, l_i, d_i, k_i) equal to the nominal values (m_o, l_o, d_o, k_o), where $m_o := m/n$ and $l_o := \ell/(2n)$. We assume that only the first joint is actuated, and the relative angle of the first joint ϕ_1 is available for feedback control.

3. Resonance analysis

We analyze resonance of the link chain with and without fluid in terms of frequency responses. Specifically, the link chain is driven by sinusoidal torque input $u(t) = a\sin\omega t$, and the responses of relative angles ϕ_i, body orientation angle θ_o, and the resulting velocity (v_x, v_y) are examined. The input amplitude is fixed to $a = 30\ \mu$Nm, which is chosen to yield reasonable amplitudes of ϕ_i. The (x,y) coordinates are chosen so that, during the steady state locomotion, the average of v_y over one cycle is zero and that of v_x is a negative value.

3.1. Verification of locomotion

Let us first verify that the link-chain locomotor can swim by converting the sinusoidal torque input to a forward velocity through the interaction with the surrounding fluid. The locomotor model (1) is simulated for a sinusoidal torque input $u(t) = a\sin\omega t$ when it is initially at rest with its body straight. The simulation result for a typical case ($\omega = 2$ Hz) is shown in Fig. 2.

Within a few cycles, the locomotion reaches the steady state where the average value of v_y is zero, that of v_x is about -0.065 m/s, and both v_x and v_y oscillate with small amplitudes. The amplitudes of ϕ_1 and ϕ_2 are about 80^o and 50^o, respectively. The phase lag of ϕ_2 with respect to ϕ_1 is about 90^o, indicating waves traveling from head to tail. The body orientation angle θ_o is also oscillating, but its amplitude is small.

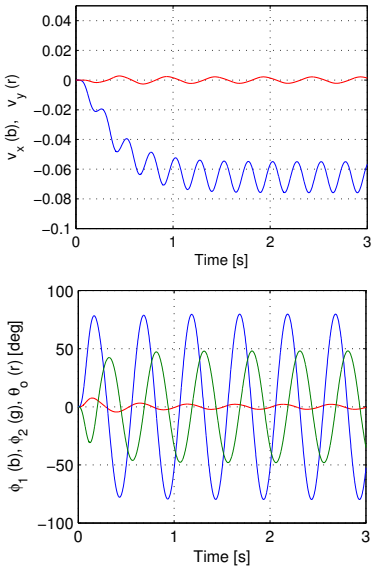

Figure 2. Time responses to $u = 30\sin(4\pi t)$ μNm

3.2. Frequency response

Anticipating that swimming of the link chain can be made efficient by exploiting a resonance, let us first study the frequency response of the body-fluid system. We consider the steady state swimming where v_x can be approximated by a constant. Using the first row of (1), the transfer function from u to ϕ_1 can then be defined as

$$P(s) := B^{\mathsf{T}}(Js^2 + Ds + \mathrm{K})^{-1}B, \tag{2}$$
$$\mathrm{K} := v_x \mathrm{c}_o F^{\mathsf{T}} + k_o C^{\mathsf{T}} C,$$

for each fixed swim speed v_x, where we noted that $F^{\mathsf{T}}e = 0$ under the uniformity assumption.

Figure 3 shows the Bode plots of $P(s)$ for several cases. The frequency response $P(j\omega)$ is shown by the red curve for the case without water ($\mathrm{c}_t = \mathrm{c}_n = 0$). The gain plot is shown as the angle output amplitude when the input torque amplitude is 30 μNm to make physical sense. The transfer function has resonance frequencies at 2.5 and 5.8 Hz, and an anti-resonance frequency at 3.2 Hz. With the fluid, the drag force adds damping and the Bode plot becomes the blue curves where the swim speed v_x is varied from 0, -0.05, to -0.1 m/s (the arrows indicate how the curves vary with v_x in this order). We see that the first resonance mode is damped by the fluid drag and no peak exists in the gain plot around 2.5 Hz. The variations in the gain and phase due to the speed change are relatively small. This insensitivity is observed for the transfer function from u to ϕ_2 as well, but not for that from u to θ_o. (The black and green curves in the phase plot will be referred to later.)

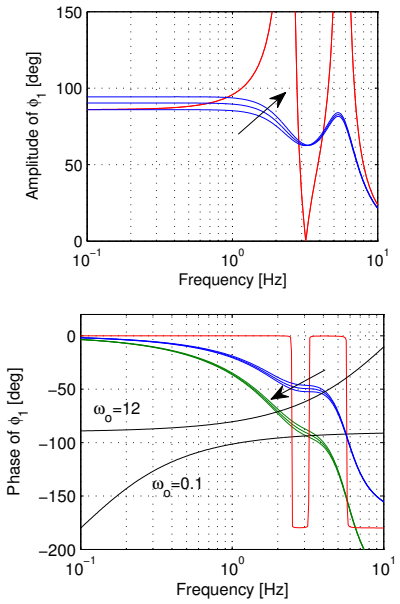

Figure 3. Frequency responses from u to ϕ_1

3.3. Resonance in swimming

Next, we examine whether there is a resonance phenomenon during swimming. We apply a sinusoidal torque input to (1) and examine how the steady state swim speed depends on the input frequency. To simplify the analysis and gain insights, let us consider the case where the velocity (v_x, v_y) varies slowly relative to the change of θ. In this case, we may regard θ as a sinusoid and (v_x, v_y) as constant over each cycle. The swim speed $|v_x|$ in the steady state, averaged over one cycle, can then be analytically estimated as described below.

Taking the average of the second and third rows of (1) over one cycle, we have

$$m\alpha_x + \frac{1}{T}\int_0^T [(n\mathrm{c}_t + \mathrm{c}_o\|\theta\|^2)v_x + \mathrm{c}_o\theta^{\mathsf{T}}F\dot{\theta}]dt = 0,$$
$$m\alpha_y + n\mathrm{c}_n v_y = 0,$$

where we noted $\int_0^T e^{\mathsf{T}}\theta dt = 0$ by definition of the (x,y) coordinates, $T := 2\pi/\omega$ is the period of oscillation, and

(α_x, α_y) is the average acceleration. The second equation indicates that v_y converges to zero in the steady state. On the other hand, the first equation can be expressed in terms of the phasor vector $\hat{\theta}$ and solved for α_x as follows:

$$\alpha_x = \frac{\hat{\theta}^* Q \hat{\theta} - (2nc_t + c_o \|\hat{\theta}\|^2) v_x}{2m}, \tag{3}$$

where $\hat{\theta}$ is a constant complex vector such that $|\hat{\theta}_i|$ and $\angle\hat{\theta}_i$ are the amplitude and phase of $\theta_i(t)$, and

$$\hat{\theta} = (\mathrm{K} - J\omega^2 + j\omega D)^{-1} Ba, \quad Q := j\omega c_o \frac{F^\mathsf{T} - F}{2}.$$

With the input amplitude $a := 30$ μNm, the acceleration α_x is plotted as a function of the velocity v_x in Fig. 4 for several values of the input frequency ω. The velocity v_x at which the acceleration α_x becomes zero is the equilibrium, where the negative slope of the v_x-α_x curve indicates its stability. Thus we have

$$v_x = \frac{\hat{\theta}^* Q \hat{\theta}}{2nc_t + c_o \|\hat{\theta}\|^2}.$$

The right hand side depends on v_x through $\hat{\theta}$, and hence this is an implicit equation. It turns out, however, that one can solve for v_x by the fixed point iteration.

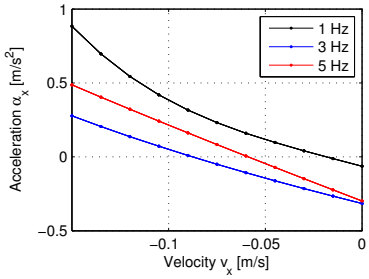

Figure 4. Acceleration-velocity relation

The swim speed $|v_x|$ thus estimated is plotted by the red curve at the top of Fig. 5. Accuracy of this estimate is confirmed by simulating the original equations of motion in (1), where the simulated speed, averaged over one cycle, is indicated by the blue curve which almost overlaps with the red curve. The amplitudes and phases of the relative angles ϕ are also plotted in Fig. 5. Clearly, there is a frequency at which the swim speed is maximum, and the peak occurs around 3 Hz. At the peak frequency, the amplitudes of ϕ_1 and ϕ_2 are about the same, and their phase difference is around 120^o. The amplitudes are not balanced if $\omega < 3$ Hz, while the phase difference gets closer to 180^o if $\omega > 3$ Hz, and both cases lead to inefficient swimming.

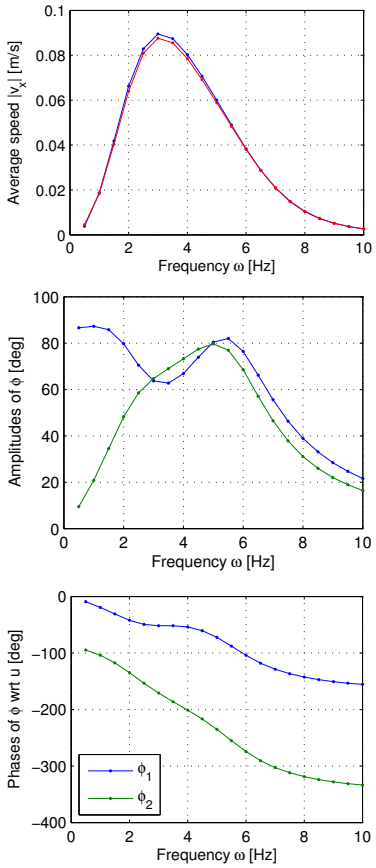

Figure 5. Frequency response of swimming locomotor

The peak frequency is close to the anti-resonance frequency $\omega_a = 3.2$ Hz of the body with (or without) fluid (see Fig. 3). To confirm that this is not a coincidence, we have considered perturbations of the masses as follows:

$$m_1 = (2r+1)m_o, \quad m_2 = m_3 = (1-r)m_o,$$

where $0 \le r < 1$. For each value of r in this interval, the undamped resonance frequencies ω_1 and ω_2, undamped anti-resonance frequency ω_a, and the frequency ω_{peak} at which the locomotion speed is maximum, are plotted in Fig. 6. Clearly, the peak frequency ω_{peak} is close to the anti-resonance frequency ω_a when $r \le 0.44$. Further calculations show that a local minimum corresponding to the anti-resonance occurs in the gain plot under the fluid damping ($|v_x| < 0.1$) at a frequency near ω_a when $r \le 0.44$, and disappears when $r > 0.44$ due to the loss of the second mode resonance peak. Thus, the peak frequency ω_{peak} is close to the undamped anti-resonance frequency ω_a whenever the gain plot under the fluid damping exhibits a corresponding local minimum.

At the anti-resonance without fluid, the first joint

angle ϕ_1 has no displacement, and the second joint oscillates at the natural frequency of the constrained two-link chain in which the first and second links are straightened and glued together. This means that the applied torque does no work on the body yet the second joint makes the "tail" flip around. With fluid, the drag adds damping and the work done by the input is no longer zero, but still the amplitude of ϕ_1 is small, making a large part of the supplied energy transferred to the tail. Thus, driving the system at the anti-resonance appears to be an efficient way to flip the tail. Even though the resonance peak at the first mode disappeared due to the fluid drag in Fig. 3, anti-resonance phenomena can still be exploited for efficient swimming.

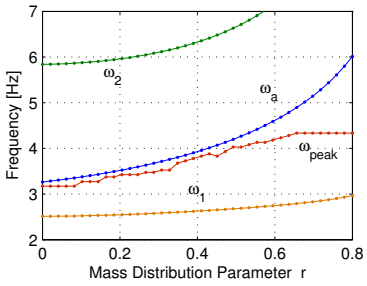

Figure 6. The peak frequency is close to the anti-resonance when it exists.

4. Feedback control by CPG

We now consider the design of feedback control systems for the link chain locomotor. The basic control unit we use is the reciprocal inhibition oscillator [6], [7] described by

$$q = f(s)(M\phi(q) + Hy), \quad u = G\phi(q),$$

$$f(s) := \frac{2\omega_o s}{(s+\omega_o)^2}, \quad \phi(q) := \tanh(q),$$

$$M := -\mu \begin{bmatrix} 0 & 1 \\ 1 & 0 \end{bmatrix}, \quad l := \begin{bmatrix} 1 \\ -1 \end{bmatrix}, \quad G := gl^{\mathrm{T}}, \quad H := hl,$$

where $\omega_o > 0$ is the intrinsic RIO frequency, $\mu > 0$ is the synaptic strength, u and y are the activation input to, and sensory output from the mechanical body, and g and h are feedback gains, respectively. The locomotor in (1) is driven by the RIO control unit with $y := \phi_1$. We use the following parameter values

$$g = 10^{-5}, \quad h = \pm 10^3, \quad \mu = 1.2,$$

and ω_o is varied within a range to see its effect on the locomotion behavior.

We approximate all the signals by sinusoids and the nonlinear function by $\phi(q) \cong \kappa q$ where κ is the describing function (amplitude dependent linear gain). Then the harmonic balance equation (HBE) is given by

$$P(j\omega)R(j\omega) = 1, \quad R(s) := \frac{2gh\kappa f(s)}{1-\mu\kappa f(s)}.$$

where $R(s)$ is the transfer function from y to u in the RIO control. The phase balance occurs when

$$\angle P(j\omega) = \angle R(j\omega)^{-1},$$

$$\begin{aligned} \angle R(j\omega)^{-1} &= \angle[gh(1-\mu\kappa+j\varpi)] \\ &\cong \begin{cases} \angle[1+j\varpi] & (gh>0) \\ \angle[1+j\varpi]-\pi & (gh<0), \end{cases} \end{aligned}$$

$$\varpi := \frac{1}{2}\left(\frac{\omega}{\omega_o} - \frac{\omega_o}{\omega}\right),$$

where κ is approximated as $\kappa \cong 0$, which is valid when $|h|$ is large, making the amplitude of q large. Thus, under a high gain feedback, the frequency of the closed-loop oscillation is predicted by the intersection of the phase curves of $P(j\omega)$ and $R(j\omega)^{-1}$. The swimming behavior can then be predicted from the frequency response curves in Fig. 3.

For the positive feedback case (Fig. 7, blue curves), the closed-loop frequency is maintained near 5 Hz when ω_o is large. The resulting swim speed is relatively high, but not always close to the peak velocity in Fig. 5. This is explained by the fact that the velocity curve in Fig. 5 goes down as the input frequency increases from 4 to 6 Hz. The phase curve $\angle(1+j\varpi)$ as a function of ω passes through the point $(\omega_o, 0)$ and approaches -90^o as ω goes to zero. The curve for the case $\omega_o = 12$ Hz is plotted in Fig. 3. The intersection with $\angle P(j\omega)$ occurs around $\omega = 4$ Hz, accurately predicting the closed-loop frequency seen in Fig. 7. As ω_o gets larger, the phase curve of $R(j\omega)^{-1}$ becomes more and more flat at -90^o, and in the limit, the intersection occurs at $\omega = 5.7$ Hz. This explains how the entrainment near 5 Hz occurs in Fig. 7. When $\omega_o \geq 12$ Hz, the HBE prediction is found accurate since the ripple in v_x is small. But when $1 \leq \omega_o \leq 8$, the ripple is large, and the effect of $\dot{v}_x$, neglected in the HBE analysis, leads to the error in the prediction. Moreover, when $9 \leq \omega_o \leq 11$, bifurcations occur and the solution does not seem even purely periodic.

For the negative feedback case (Fig. 7, black curves), entrainment to 5.7 Hz occurs when ω_o is small. This is also explained by the HBE analysis. The phase curve $\angle(1+j\varpi)-\pi$ is plotted in Fig. 3 for the case $\omega_o = 0.1$ Hz. The intersection with the blue curve occurs a little below 6 Hz, accurately predicting the

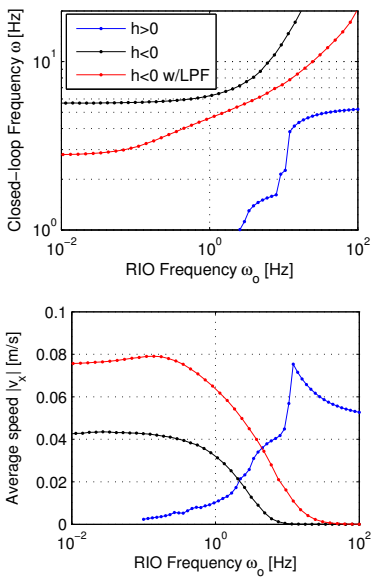

Figure 7. Steady state locomotion of the link chain driven by RIO

closed-loop frequency. When ω_o is sufficiently small, we have $\angle(1+j\varpi)-\pi \cong -\pi/2$, and the intersection is around 5.7 Hz, explaining the entrainment.

For neither the positive nor negative feedback case, is entrainment to the resonance peak velocity achieved, as seen in Fig. 5. In view of the figure, the resonance entrainment occurs when the phase balance occurs around 3 Hz. Since the phase of $P(j\omega)$ is about -50^o at 3 Hz (Fig. 3), the RIO frequency ω_o should be chosen so that the phase of $R(j\omega)^{-1}$ is also -50^o at 3 Hz. This can be achieved, not by negative feedback, but by positive feedback with $\omega_o \cong 8$ Hz. However, if ω_o is 8 Hz or a little smaller, then the ripples in v_x makes the HBE prediction inaccurate and the peak speed (0.09 m/s) is not attained. If ω_o is slightly above 8 Hz, then stable oscillations are not obtained. Thus, the RIO control cannot achieve anti-resonance entrainment.

Entrainment to the anti-resonance can be induced by inserting a low pass filter

$$W(s) := \frac{a}{1+\tau s}, \quad \tau = \frac{1}{7\pi}, \quad a = \sqrt{2}.$$

in the sensory feedback path so that $y = W(s)\phi_1$. The effect is to reduce the phase by 45^o at $\omega = 1/\tau = 3.5$ Hz while keeping the same gain. As a result, the phase of $W(j\omega)P(j\omega)$ becomes about -90^o around the anti-resonance frequency 3 Hz, and the RIO control with negative feedback achieves entrainment to the anti-resonance when ω_o is sufficiently small (Fig. 7, red curves).

5. Conclusion

We have studied an underactuated three-link swimming locomotor and obtained the following results. Contrary to a common expectation, the most efficient swimming is achieved when the input frequency is close to the anti-resonance, rather than a resonance. Although previous results indicated that the RIO can entrain to the resonance of a simple pendulum, the RIO is not able to entrain to the first mode resonance nor the anti-resonance of the locomotor due to the additional effect of the fluid force. However, the anti-resonance entrainment can be achieved by inserting a phase-lag compensator in the feedback loop.

Acknowledgments: The authors gratefully acknowledge the supports from the Office of Naval Research, under MURI Grant N00014-08-1-0642, and from the National Science Foundation under No.0654070. They also thank Prof. W.O. Friesen and Ms. J. Chen for providing parameter values of a typical leech used in this study.

References

[1] W.B. Kristan Jr., R. Calabrese, and W.O. Friesen. Neuronal control of leech behavior. *Prog. in Neurobiol.*, 76:279–327, 2005.

[2] N.G. Hatsopoulos. Coupling the neural and physical dynamics in rhythmic movements. *Neural Computation*, 8(3):567–581, 1996.

[3] M.M. Williamson. Neural control of rhythmic arm movements. *Neural Networks*, 11:1379–1394, 1998.

[4] B.W. Verdaasdonk, H.F. Koopman, and F.C. Van der Helm. Energy efficient and robust rhythmic limb movement by central pattern generators. *Neural Network*, 19(4):388–400, 2006.

[5] B.W. Verdaasdonk, H.F. Koopman, and F.C. Van der Helm. Resonance tuning in a neuro-musculoskeletal model of the forearm. *Biological Cybernetics*, 96(2):165–180, 2007.

[6] T. Iwasaki and M. Zheng. Sensory feedback mechanism underlying entrainment of central pattern generator to mechanical resonance. *Biological Cybernetics*, 94(4):245–261, 2006.

[7] Y. Futakata and T. Iwasaki. Formal analysis of resonance entrainment by central pattern generator. *J. Math. Biol.*, 57(2):183–207, 2008.

[8] W.O. Friesen. Reciprocal inhibition: A mechanism underlying oscillatory animal movements. *Neurosci. and Biobehav. Rev.*, 18(4):547–553, 1994.

[9] M. Saito, M. Fukaya, and T. Iwasaki. Serpentine locomotion with robotic snake. *IEEE Control Systems Magazine*, 22(1):64–81, 2002.

[10] G. Taylor. Analysis of the swimming of long and narrow animals. *Proc. Royal Society of London. Series A*, 214(1117):158–183, 1952.